Published in "Neuron 57(4): 536-545, 2008"
which should be cited to refer to this work.

Nanodomain Coupling between Ca^{2+} Channels and Ca^{2+} Sensors Promotes Fast and Efficient Transmitter Release at a Cortical GABAergic Synapse

Iancu Bucurenciu,[1] Akos Kulik,[2] Beat Schwaller,[3] Michael Frotscher,[2] and Peter Jonas[1,*]
[1]Physiological Institute I, University of Freiburg, Hermann-Herder-Strasse 7, D-79104 Freiburg, Germany
[2]Institute of Anatomy and Cell Biology, University of Freiburg, Albertstrasse 17, D-79104 Freiburg, Germany
[3]Unit of Anatomy, Department of Medicine, University of Fribourg, 1 Route Albert-Gockel, CH-1700 Fribourg, Switzerland
*Correspondence: peter.jonas@physiologie.uni-freiburg.de

SUMMARY

It is generally thought that transmitter release at mammalian central synapses is triggered by Ca^{2+} microdomains, implying loose coupling between presynaptic Ca^{2+} channels and Ca^{2+} sensors of exocytosis. Here we show that Ca^{2+} channel subunit immunoreactivity is highly concentrated in the active zone of GABAergic presynaptic terminals of putative parvalbumin-containing basket cells in the hippocampus. Paired recording combined with presynaptic patch pipette perfusion revealed that GABA release at basket cell-granule cell synapses is sensitive to millimolar concentrations of the fast Ca^{2+} chelator BAPTA but insensitive to the slow Ca^{2+} chelator EGTA. These results show that Ca^{2+} source and Ca^{2+} sensor are tightly coupled at this synapse, with distances in the range of 10–20 nm. Models of Ca^{2+} inflow-exocytosis coupling further reveal that the tightness of coupling increases efficacy, speed, and temporal precision of transmitter release. Thus, tight coupling contributes to fast feedforward and feedback inhibition in the hippocampal network.

INTRODUCTION

The distance between presynaptic Ca^{2+} channels and the Ca^{2+} sensor of exocytosis is a key factor that determines the efficacy and timing of synaptic transmission. Although this distance is difficult to measure directly, it can be probed by exogenous Ca^{2+} chelators (Adler et al., 1991). This approach has been applied previously to a variety of synapses. In the squid giant synapse, transmitter release is suppressed by millimolar concentrations of the fast Ca^{2+} chelator BAPTA but is unaffected by 80 mM of the slow Ca^{2+} chelator EGTA (Adler et al., 1991), indicating that the diffusional distance between Ca^{2+} source and Ca^{2+} sensor is in the nanometer range (Neher, 1998). In contrast, in the young calyx of Held and in neocortical glutamatergic synapses, transmitter release is suppressed by both 1 mM BAPTA and 1 mM EGTA (Borst and Sakmann, 1996; Meinrenken et al., 2002; Fedchyshyn and Wang, 2005; Ohana and Sakmann, 1998; Rozov et al., 2001), suggesting that that the source-sensor distance must be longer, close to the micrometer range (Meinrenken et al., 2002). These results led to the prevailing view that transmitter release at the squid giant synapse is triggered by Ca^{2+} nanodomains, whereas release at central synapses in the mammalian cortex is initiated by Ca^{2+} microdomains in presynaptic terminals (Augustine et al., 2003).

However, whether these conclusions apply generally to central synapses in the mammalian brain has remained unclear. As tight coupling between Ca^{2+} channels and synaptic vesicles is expected to minimize the diffusional component of the synaptic delay (Meinrenken et al., 2002), it is possible that the distance between Ca^{2+} source and Ca^{2+} sensor is particularly short in neuron types specialized for rapid signaling. To test this idea, we probed the spatial relation between Ca^{2+} source and Ca^{2+} sensor at the output synapses of fast-spiking, parvalbumin-expressing GABAergic basket cells (BCs) in the dentate gyrus of the hippocampus. These neurons operate as fast signaling devices, generating rapid and temporally precise inhibitory synaptic output signals onto postsynaptic target cells (Jonas et al., 2004; Bartos et al., 2007; Freund and Katona, 2007). We found that the distance between Ca^{2+} source and Ca^{2+} sensor at these synapses is in the nanometer range, similar to the squid giant synapse (Adler et al., 1991), but very different from any other previously studied cortical synapse.

RESULTS

Ca^{2+} Channel Immunoreactivity Is Clustered in Active Zones of BC Synapses

We explored the possibility that tight coupling between Ca^{2+} source and Ca^{2+} sensor may contribute to the fast signaling at the basket cell (BC)-granule cell (GC) synapse in the dentate gyrus. As previous studies showed that transmitter release at this synapse is entirely mediated by P/Q-type Ca^{2+} channels (Hefft and Jonas, 2005; see Poncer et al., 1997; Wilson et al., 2001), we first examined the distribution of α_{1A} subunit immunoreactivity on putative BC terminals by high-resolution immunoelectron microscopy (Figure 1). BC terminals were identified by the symmetrical contacts that they formed on granule cell somata. Pre-embedding immunogold labeling revealed that α_{1A} immunoreactivity was highly concentrated in the active zone of putative BC terminals. In both adjacent serial sections (Figures 1A and 1B) and in three-dimensionally reconstructed boutons

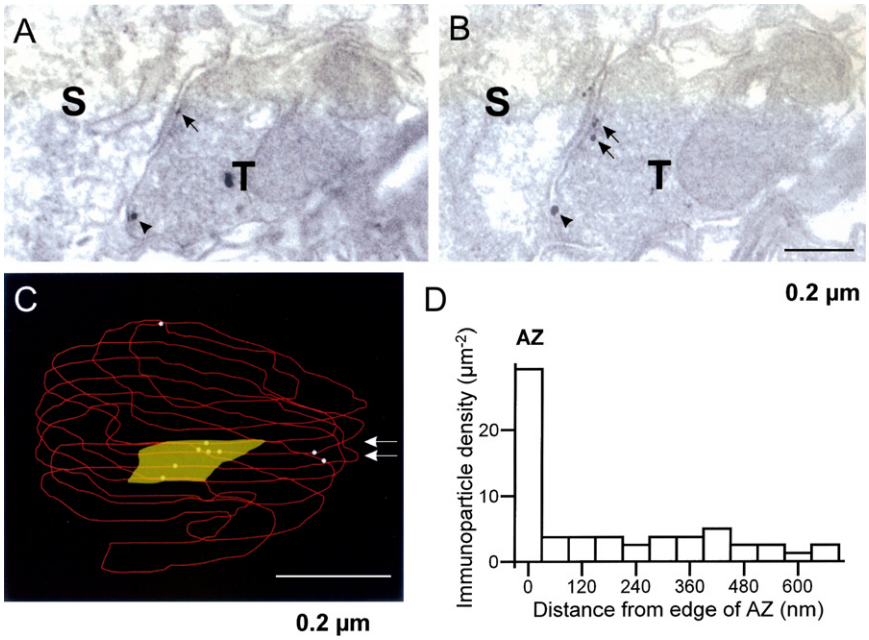

Figure 1. α_{1A} Subunit Immunoreactivity Is Concentrated in the Active Zone of Putative BC Terminals

(A and B) Electron micrographs showing a presynaptic terminal (T) in consecutive ultrathin sections that establishes a symmetrical synaptic contact with a neuronal soma (S) in the granule cell layer of the dentate gyrus. Pre-embedding immunogold labeling revealed that α_{1A} immunoreactivity was mainly localized at the presynaptic membrane specialization (arrows); immunogold particles were only occasionally seen on the extrasynaptic plasma membrane (arrowheads) of boutons. Note that the particles were present at similar locations in adjacent sections.

(C) Three-dimensional reconstruction of the same axon terminal (arrows point to the sections shown in [A] and [B]). Reconstruction was carried out from serial ultrathin sections (n = 9) obtained from pre-embedding material showing the localization of immunogold particles for α_{1A} (white dots) in relation to the active zone (yellow area).

(D) Histogram showing the density of immunogold particles (n = 54) for α_{1A} on presynaptic terminals (n = 11) in the region of the active zone (AZ) and in extrasynaptic membranes. For the extrasynaptic region, distances of immunogold particles were measured from the closest edge of AZs along the surface of the reconstructed boutons. Density was determined by counting the number of particles and dividing it by the respective surface area of the presynaptic membrane. Scale bars, 0.2 µm.

(Figure 1C), immunogold particles were mainly found in the active zone. Analysis of particle density on the plasma membrane in 92 ultrathin sections from 11 putative BC terminals revealed that the particle density (n = 54) was 9-fold higher in the active zone than in the extrasynaptic membrane of the presynaptic terminal (29.2 ± 7.4 μm^{-2} versus 3.2 ± 0.3 μm^{-2}; $p < 0.01$; Figure 1D). These results suggest that P/Q-type Ca^{2+} channels, the presynaptic Ca^{2+} sources for transmitter release at BC output synapses (Hefft and Jonas, 2005), are highly concentrated in the active zone, consistent with a tight coupling of these channels to the exocytotic machinery.

Transmitter Release Is Inhibited by the Fast Ca^{2+} Chelator BAPTA, but Insensitive to the Slow Chelator EGTA

To quantify the distance between Ca^{2+} source and Ca^{2+} sensor, we tested the effect of exogenous chelators on transmitter release at BC-GC synapses (Adler et al., 1991). Unitary IPSCs were measured in the paired recording configuration, and Ca^{2+} chelators were loaded into presynaptic interneurons at defined concentrations by patch pipette perfusion (Figure 2A and Figure S1). Pipette perfusion allowed us to exchange the solution at the tip of the patch pipette within ~2 min (Figure 2C). To estimate the time required to load chelators into presynaptic terminals, we simulated chelator diffusion in a detailed model of BC morphology in which the soma, dendrites, and proximal axon were reconstructed and the axon was schematically extended with 150 collaterals. Simulation of diffusion revealed that the chelator concentration in axon collaterals reached 76%–99% of the somatic concentration after 100 min, with faster exchange in proximal than in distal collaterals (Figure 2D). Thus, chelators can be loaded into presynaptic terminals within typical recording times if these presynaptic terminals emerge from proximal axon collaterals.

We next examined the effects of Ca^{2+} chelators in BC-GC paired recordings with <100 µm intersomatic distance to minimize diffusion times (Figure 2A). The effect of Ca^{2+} chelators was quantified as the ratio of $IPSC_{chelator}/IPSC_{control}$, where $IPSC_{control}$ was measured during a 7.5 min control period and $IPSC_{chelator}$ was determined from a 7.5 min test period after stationary effects were reached (on average 85 min after application onset). Loading the presynaptic BC with 10 mM of the fast Ca^{2+} chelator BAPTA reduced the amplitude of unitary BC-GC IPSCs substantially. On average, the peak amplitude of the unitary BC-GC IPSCs under steady-state conditions was 16.3% ± 3.6% of the control value (five pairs; Figures 3A and 3B). Conversely, in cells preloaded with 10 mM BAPTA, the application of BAPTA-free intracellular solution led to a time-dependent increase of the IPSC amplitude (Figures 3C and 3D), suggesting reversibility of the prior effects of BAPTA on transmitter release. On average, the ratio of unitary BC-GC IPSC amplitude after 90 min to the minimal amplitude ~20 min after solution exchange was 2.5 ± 0.2 (three pairs). Collectively, these results indicate that 10 mM of the fast Ca^{2+} chelator BAPTA consistently and reversibly inhibited synaptic transmission at the BC-GC synapse.

In contrast, loading the presynaptic BC with 30 mM of the slow Ca^{2+} chelator EGTA reduced the amplitude of the evoked IPSC to only 67.2% ± 4.3%, markedly less than 10 mM BAPTA (five pairs; $p < 0.01$; Figures 4A and 4B). We further attempted to determine the half-maximal inhibitory concentration of the chelator effects. For BAPTA, the effects were concentration dependent; 1, 3, 10, and 30 mM BAPTA decreased the IPSC amplitude to 63.7%, 32.3%, 16.3%, and 1.6% of the control value (15 pairs total; $p < 0.001$), yielding a half-maximal inhibitory concentration of 1.6 mM (Figure 4C). For EGTA, a concentration-effect relation could not be obtained, because even high concentrations of

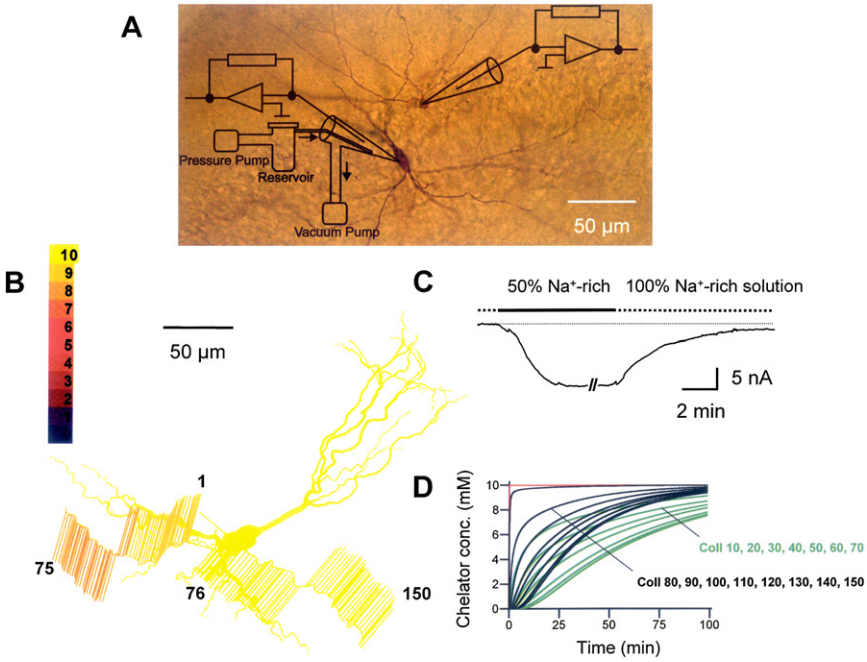

Figure 2. Loading of Ca^{2+} Chelators into Presynaptic Terminals of BCs via Somatic Pipette Perfusion

(A) Photomicrograph of a BC-GC pair, filled with biocytin, stained using 3,3′-diaminobenzidine, and examined light-microscopically. Patch pipettes and pipette perfusion apparatus are superimposed schematically.

(B) Model of BC morphology used for simulation of chelator diffusion. Pseudocolor representation (inset) shows the chelator concentration after 100 min. The BC model was taken from Geiger et al. (1997).

(C) Speed of solution exchange at the pipette tip, measured as a change in junction current in an open patch pipette during a solution change from 100% Na^+-rich to 50% Na^+-rich solution and back via pipette perfusion.

(D) Simulation of the chelator concentration in 15 axon collaterals as a function of time (green curves, collaterals 10–70; black curves, collaterals 80–150; red curve, concentration at the soma; indices of collaterals correspond to the numbers in [B]). 100 min after a somatic concentration jump, the chelator concentration in the axon collaterals reaches between 99% and 76% of the somatic concentration.

EGTA had only moderate effects. However, assuming that the concentration dependence follows a Hill equation with a Hill coefficient of 1, the half-maximal inhibitory concentration was estimated as ~61.5 mM. Thus, the ratio of half-maximal inhibitory concentrations between BAPTA and EGTA (~38) is similar to the inverse ratio of the Ca^{2+} binding rates of the chelators (~40; Nägerl et al., 2000; Naraghi and Neher, 1997; Neher, 1998).

To reassure that the effects of Ca^{2+} chelators were generated at a presynaptic site, we tested possible effects on the number of failures and the coefficient of variation, indicators of presynaptic changes (Figure S2). BAPTA significantly increased the percentage of transmission failures ($p < 0.001$; Figures S2A and S2B) and reduced the coefficient of variation of IPSC peak amplitudes raised to the power of −2 ($p < 0.001$; Figure S2C), confirming that the chelator effects were generated at a presynaptic locus.

The Exocytotic Ca^{2+} Sensor at the BC-GC Synapse Is Not Saturated

The relative insensitivity of transmitter release at BC terminals to exogenous Ca^{2+} chelators, in particular to the slow Ca^{2+} chelator

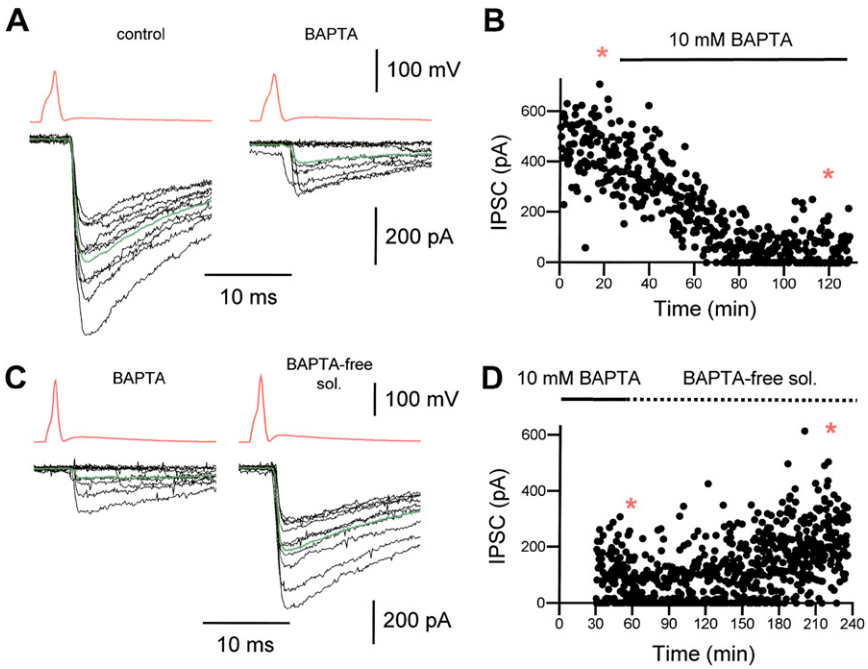

Figure 3. Transmitter Release at the BC-GC Synapse Is Reversibly Inhibited by 10 mM of the Fast Ca^{2+} Chelator BAPTA

(A) Presynaptic action potentials (red) and evoked IPSCs (black) under control conditions (left) and after application of 10 mM BAPTA (right). Ten consecutive traces are shown superimposed; the average IPSC is shown in green.

(B) Plot of IPSC peak amplitude against time during application of BAPTA via presynaptic patch pipette perfusion. Same pair as shown in (A). Time of application of 10 mM BAPTA is represented by the horizontal bar. Asterisks indicate the times at which traces in (A) were taken.

(C and D) Similar recording as in (A) and (B), but before and after a change from 10 mM BAPTA-containing to BAPTA-free intracellular solution. Note the increase in amplitude of evoked IPSCs, indicating reversibility of the prior effect of BAPTA.

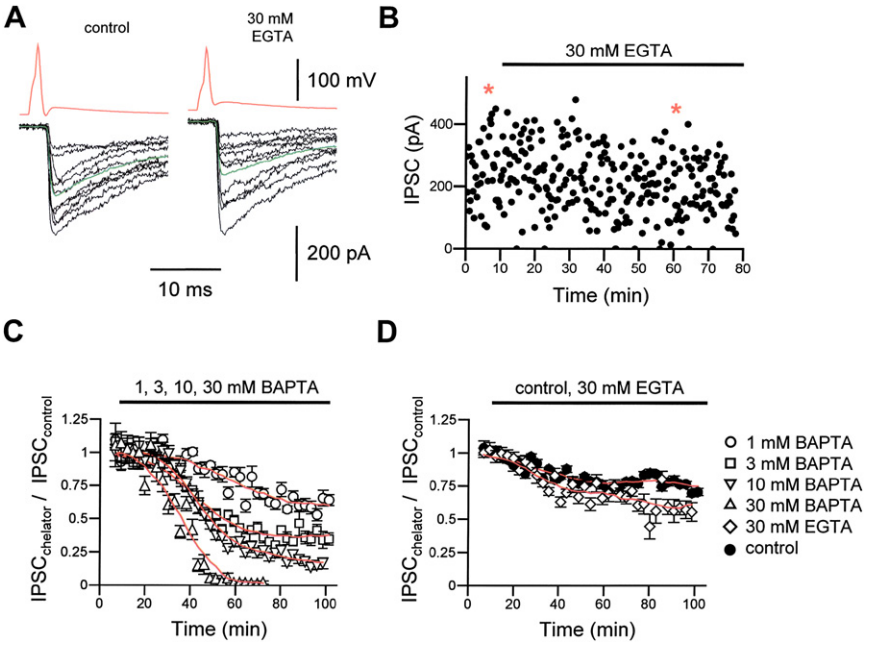

Figure 4. Transmitter Release at the BC-GC Synapse Is Resistant to the Slow Ca^{2+} Chelator EGTA

(A) Presynaptic action potentials and evoked IPSCs under control conditions (left) and after application of 30 mM EGTA to the presynaptic BC by pipette perfusion (right). Ten consecutive traces are shown superimposed; the average IPSC is shown in green.

(B) Plot of IPSC peak amplitude against time during application of EGTA. Same cell as shown in (A). Time of application of 30 mM EGTA is represented by the horizontal bar. Asterisks indicate the times at which traces in (A) were taken.

(C) Time course of the onset of the effect of 1 (circles), 3 (squares), 10 (inverted triangles), and 30 mM BAPTA (triangles). Data from four, four, five, and two pairs were aligned to the onset time of the BAPTA application, normalized to the control amplitude, condensed by forming means of ten adjacent data points, and averaged across pairs.

(D) Time course of the onset of the effect of 30 mM EGTA (diamonds) and control solution (mock application, filled circles). Data from five and four pairs, respectively. Note that EGTA has small, but detectable effects. The red curves in (C) and (D) represent sliding averages.

Error bars indicate SEM.

EGTA, suggests a tight coupling between Ca^{2+} source and Ca^{2+} sensor. Alternatively, the relative insensitivity may be explained by saturation of the sensor during presynaptic Ca^{2+} transients. In this scenario, changes in presynaptic Ca^{2+} inflow would not lead to corresponding changes in transmitter release. We therefore examined the possibility of saturation of the presynaptic Ca^{2+} sensor by varying the extracellular Ca^{2+} concentration between 0.5 and 4 mM, while keeping the extracellular Mg^{2+} concentration constant (Figure 5). Reduction of the external Ca^{2+} concentration below the control value of 2 mM resulted in a marked decrease in IPSC peak amplitude and a parallel increase in the proportion of failures. Conversely, increase in the external Ca^{2+} concentration above 2 mM resulted in an increase in IPSC peak amplitude beyond the control value. Analysis of the quantitative relation between IPSC amplitude and extracellular Ca^{2+} concentration revealed that the half-maximal effective concentration of Ca^{2+} was 1.76 mM (Figure 5C). Thus, the degree of saturation of the Ca^{2+} sensor for 2 mM Ca^{2+} was

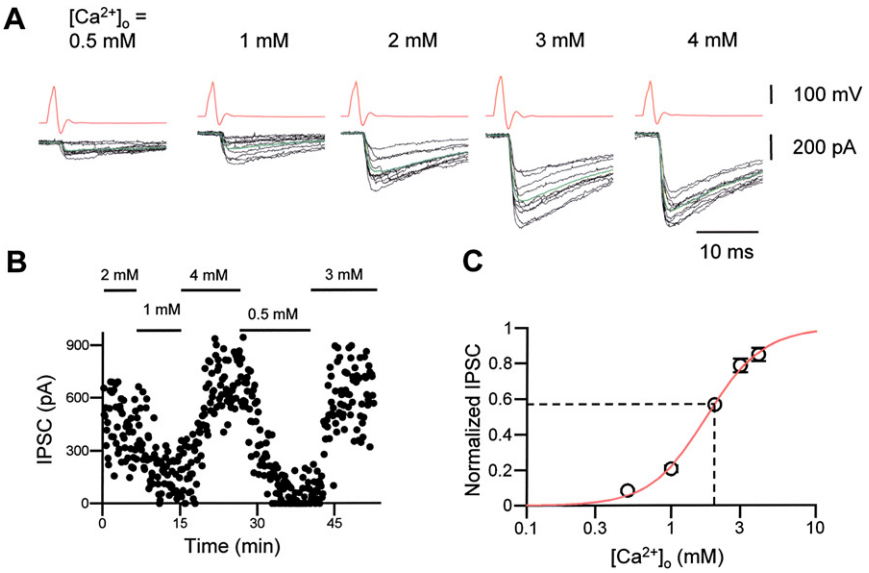

Figure 5. The Exocytotic Ca^{2+} Sensor at BC-GC Synapses Is Not Saturated by Presynaptic Ca^{2+} Inflow

(A) Presynaptic action potentials (red) and evoked IPSCs (black) under control conditions (center, 2 mM extracellular Ca^{2+}) and in the presence of different extracellular Ca^{2+} concentrations, as indicated on top. The extracellular Mg^{2+} concentration was held constant at 1 mM. Ten consecutive traces are shown superimposed; the average IPSC is shown in green.

(B) Plot of IPSC peak amplitude against time during application of extracellular solutions with different Ca^{2+} concentrations. Same pair as shown in (A). The time of application of the different extracellular solutions is represented by horizontal bars.

(C) Relation between IPSC amplitude and extracellular Ca^{2+} concentration. IPSC peak amplitudes were normalized to the value at 2 mM extracellular Ca^{2+}, averaged across pairs, fitted with the function $f([Ca]) = f_{max}\,[1 + (K/[Ca])^n]^{-1}$, yielding parameter values of f_{max} = 1.76, K = 1.76 mM, and n = 2.23, and renormalized to f_{max}. Red curve, normalized fitted function; dashed lines, normalized IPSC amplitude at 2 mM extracellular Ca^{2+}, indicating that the Ca^{2+} sensor showed 57% saturation. Data from five to seven pairs for each concentration. Error bars indicate SEM.

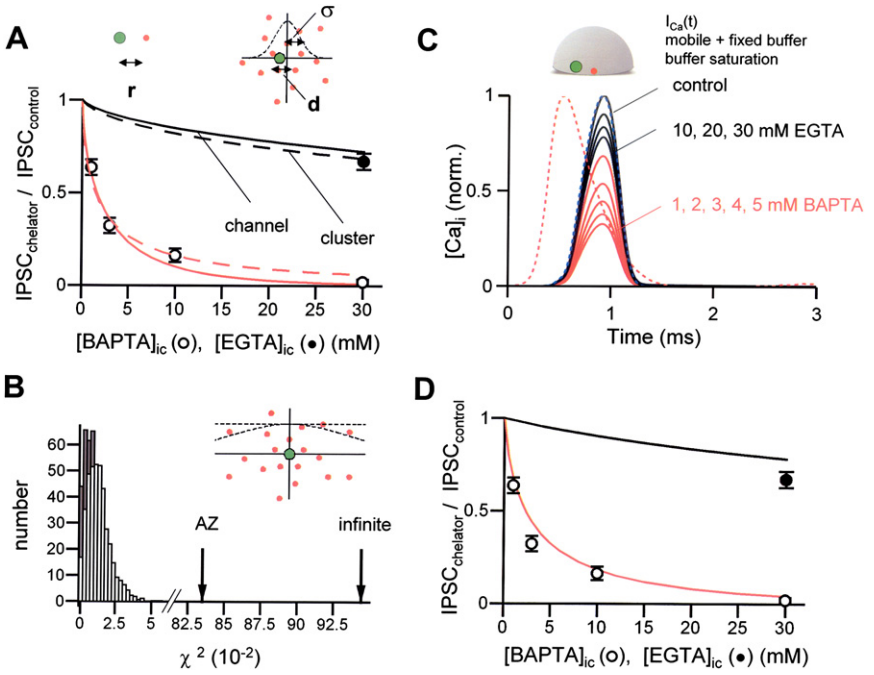

Figure 6. Concentration Dependence of BAPTA and EGTA Effects Suggests Nanodomain Coupling between Ca^{2+} Source and Ca^{2+} Sensor

(A and B) Analysis of the chelator effects using the analytical steady-state solution to the linearized reaction-diffusion equations. (A) Plot of ratio of IPSC peak amplitude in the presence of chelator to that in control conditions against the concentration of BAPTA (open symbols) or EGTA (filled symbol). Curves represent the predictions of the models fit to the entire data set (continuous curve, single-channel model; dashed curve, cluster model). Schematic illustration of the models is shown on top (red dots, Ca^{2+} channels; green dot, synaptic vesicle with Ca^{2+} sensor). The best fit parameters were r = 12 nm (single-channel model) and d = 12 nm with σ = 8 nm (cluster model).

(B) Both the single-channel and the cluster model fit the experimental data substantially better than models with more homogeneous Ca^{2+} sources. Histograms of the sum of squared differences between data and model (χ^2) for 1000 bootstrap replications of the original data fitted with either the single-channel model (open bars) or the cluster model (filled bars). Arrows indicate the χ^2 values of models in which the size of the Ca^{2+} channel cluster σ corresponds to the average radius of an active zone (174 nm; "AZ") or in which the Ca^{2+} channels were homogeneously distributed over the entire bouton area ("infinite").

(C and D) Analysis of the chelator effects using the time-dependent solution to the full reaction-diffusion equations, considering mobile and fixed buffers as well as buffer saturation. Data were obtained as the numerical solution of Equations 5–7. (C) Ca^{2+} transients at 20 nm distance from the source under control conditions (upper black line) and in the presence of different concentrations of EGTA (lower black lines) or BAPTA (red lines). Dashed red line, normalized presynaptic action potential; dashed blue line, normalized presynaptic Ca^{2+} current.

(D) Concentration dependence of the chelator effects, analyzed with the time-dependent solution to the full reaction-diffusion equations. Curves represent the predictions of the fitted model with r = 17 nm. Error bars indicate SEM.

57%, implying that the sensor operates in a subsaturating regime. These results corroborate the conclusion that the relative insensitivity against exogenous Ca^{2+} chelators at the BC-GC synapse is caused by tight coupling of source and sensor rather than saturation of the sensor.

The Distance between Ca^{2+} Source and Ca^{2+} Sensor Is in the Nanometer Range

To quantify the distance between Ca^{2+} source and Ca^{2+} sensor at the BC-GC synapse, we modeled the concentration dependence of the effects of BAPTA and EGTA on BC-GC IPSCs (Figure 6). The ratio of Ca^{2+} concentrations at the sensor in the presence and absence of exogenous chelator was modeled using the analytical steady-state solution to the linearized reaction-diffusion equations (Neher, 1998), and the corresponding ratio of IPSC amplitudes was predicted using the experimentally determined relation between Ca^{2+} concentration and transmitter release (Figure 5C).

We first examined the simplest possible model in which a single Ca^{2+} channel was coupled to the Ca^{2+} sensor (i.e., the vesicle) at variable distance r (single-channel model; Figure 6A) (Stanley, 1993, 1997; Brandt et al., 2005; Shahrezaei et al., 2006). We further tested a more complex model in which a cluster of Ca^{2+} channels, represented by a normally distributed channel density with standard deviation σ, was coupled to the Ca^{2+} sensor located at variable distance d from the cluster center (cluster model; Figure 6A). The diffusion coefficient of Ca^{2+}, the physicochemical properties of the chelators, the biological properties of the endogenous buffer, and the resting Ca^{2+} concentration in BCs (Y. Aponte et al., 2006, Soc. Neurosci., abstract; Lee et al., 2000) were experimentally constrained (Experimental Procedures), leaving r or d and σ as free parameters.

The single-channel model provided an adequate fit to the experimental observations; r was estimated as 12 ± 1 nm under these conditions. The cluster model also described the experimental data; d was estimated as 12 ± 4 nm and σ as 8 ± 5 nm. The values obtained for the source-sensor distance were insensitive to variations in the assumed biological parameters; a 10-fold decrease or increase in the endogenous buffer product changed r by −3 and 10%, and a 3-fold decrease or increase in the resting Ca^{2+} concentration changed r by −10 and 25%, respectively. We also tested whether models in which Ca^{2+} channels were normally distributed over the entire active zone (radius 174 nm) or homogeneously distributed over the entire bouton area were able to describe the chelator effects. However, we found that these models were inconsistent with the experimental observations ($p < 0.001$; Figure 6B).

To test whether similar estimates of the coupling distance between Ca^{2+} source and Ca^{2+} sensor are obtained in a more detailed model that takes into account both coexistence of

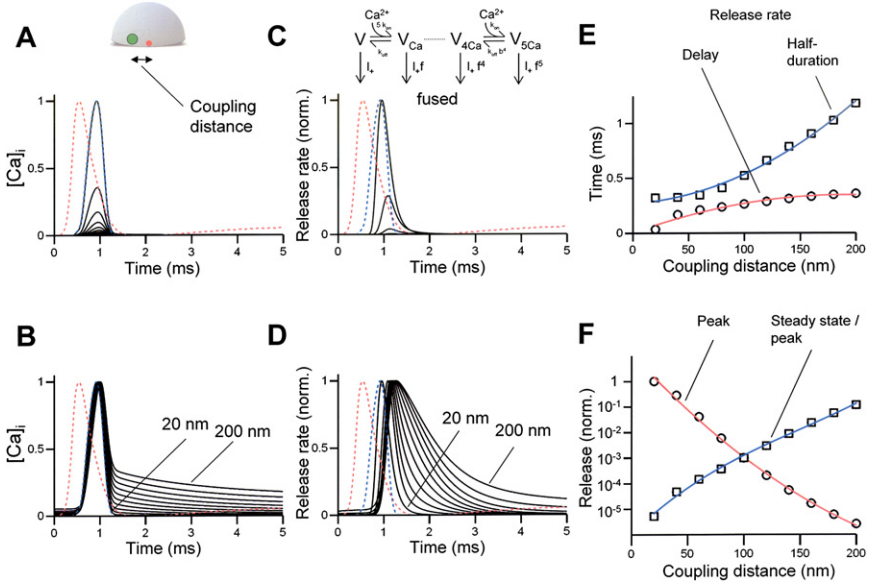

Figure 7. Tight Coupling Increases Efficacy, Speed, and Temporal Precision of Transmitter Release at BC Output Synapses

(A and B) Ca^{2+} transients at different distances from the source (20–200 nm, 20 nm increment). Ca^{2+} transients (black lines) were calculated using the time-dependent solution to the full reaction-diffusion equations (Equations 5–7; see inset). In (A), all Ca^{2+} transients were normalized to the same peak value at 20 nm. In (B), all Ca^{2+} transients were normalized to their individual peak values.

(C and D) Release rate for different source-sensor distances (20–200 nm, 20 nm increment). Release rates (black lines) were calculated from the Ca^{2+} transients using a 12 state transmitter release model (inset). In (C), all release rates were normalized to the same peak value at 20 nm. In (D), all release rates were normalized to their individual peak values.

In (A)–(D), the dashed red lines represent the normalized presynaptic action potential, and the dashed blue lines indicate the normalized presynaptic Ca^{2+} current.

(E) Plot of delay from the peak of the Ca^{2+} current to the maximal release rate (circles, red line) and half-duration of the release period (squares, blue line) against coupling distance. Tight coupling decreases the synaptic delay and the half-duration of the release period.

(F) Semilogarithmic plot of peak release rate (circles, red line, normalized to the peak release rate at 20 nm) and ratio of release rate in the steady state (at 5 ms)/release rate at the peak (squares, blue line) against coupling distance. Tight coupling increases the peak release rate and decreases the proportion of asynchronous release. Lines in (E) and (F) represent fits with polynomial functions.

mobile and immobile buffers and buffer saturation, we further modeled the concentration dependence of the chelator effects using the time-dependent solution of the full reaction-diffusion equations obtained numerically (Figures 6C and 6D) (Smith, 2001). In a single-channel scenario, the model adequately described the experimental observations with a coupling distance of 17 nm. Thus, independently of the details of the model, the coupling distance between Ca^{2+} source and Ca^{2+} sensor at the BC-GC synapse is 10–20 nm, comparable to the squid giant synapse, but much tighter than at any other cortical synapse studied to date.

Tight Coupling Enhances Efficacy, Speed, and Temporal Precision of Transmitter Release

To address the functional significance of tight coupling for fast inhibitory synaptic transmission, we simulated Ca^{2+} transients at various distances from the Ca^{2+} source, using the time-dependent solution to the full reaction-diffusion equations (Figure 7). For a bouton of 0.5 μm radius, the peak Ca^{2+} steeply declined as a function of distance, as expected for diffusion from a point source (Figure 7A). Furthermore, with increasing distance from the source, the ratio of Ca^{2+} at the peak to that at later times decreased substantially (Figure 7B). Thus, tight coupling between Ca^{2+} source and Ca^{2+} sensor increases the peak amplitude of the Ca^{2+} transient, while decreasing the relative amplitude of the Ca^{2+} concentration at later times in the presynaptic terminals.

To examine how the tightness of coupling affects transmitter release, we further modeled the corresponding release rates using a Ca^{2+} sensor model with five Ca^{2+} binding sites (Figures 7C and 7D; Lou et al., 2005). Increasing the distance between source and sensor from 20 to 200 nm increased the synaptic delay (measured from the rise of the presynaptic action potential to the peak release rate) 1.57-fold from 560 to 880 μs and increased the half-duration of the time course of release 3.66-fold (Figures 7D and 7E). Thus, tight coupling between Ca^{2+} source and Ca^{2+} sensor increases both speed and temporal precision of transmitter release at BC output synapses. Furthermore, increasing the distance between source and sensor from 20 to 200 nm substantially reduced synchronous release (measured as the peak release rate) but reduced asynchronous release (measured at t = 5 ms) to a much smaller extent, leading to a relative enhancement of asynchronous components (Figures 7D and 7F). As the coupling distance was increased from 20 to 200 nm, the ratio of asynchronous to synchronous release rate increased ~20,000-fold. Thus, tight coupling between Ca^{2+} source and Ca^{2+} sensor increases the speed and temporal precision of synaptic transmission, while reducing the relative contribution of asynchronous release.

DISCUSSION

We found that P/Q-type Ca^{2+} channels are concentrated at the active zone of putative BC terminals and that transmitter release at BC-GC synapses is surprisingly resistant to Ca^{2+} chelators. The most likely explanation of this result is a tight coupling between the Ca^{2+} source and the Ca^{2+} sensor of exocytosis. Alternative explanations, such as saturation of the exocytotic Ca^{2+} sensor or a high endogenous Ca^{2+} buffer capacity of BCs, are unlikely. Saturation of the Ca^{2+} sensor during synaptic transmission (caused for example by the high affinity of the sensor) is incompatible with the experimentally determined relation between IPSC amplitude and extracellular Ca^{2+} concentration, which further increases as the Ca^{2+} concentration is raised

above the physiological value of 2 mM. High endogenous buffer capacity is also unlikely, since the somatodendritic endogenous Ca^{2+} binding ratio of fast-spiking BCs in the dentate gyrus is ~200 (Y. Aponte et al., 2006, Soc. Neurosci., abstract; Lee et al., 2000; Collin et al., 2005), ~20-fold lower than the exogenous Ca^{2+} binding ratio of 1 mM BAPTA (κ ~concentration/dissociation constant = 1000 μM/0.22 μM ~4500) (Neher, 1998). Thus, tight coupling between the presynaptic Ca^{2+} channels and the exocytotic Ca^{2+} sensors is the only interpretation consistent with all experimental observations.

With respect to the tight coupling between Ca^{2+} source and Ca^{2+} sensor, the BC-GC synapse is similar to the squid giant synapse (Adler et al., 1991) but different from any other cortical synapse studied to date (Ohana and Sakmann, 1998; Rozov et al., 2001). The BC-GC synapse also differs markedly from the young calyx of Held (Borst and Sakmann, 1996; Meinrenken et al., 2002), although a developmental increase in the tightness of coupling between Ca^{2+} channels and transmitter release was suggested (Fedchyshyn and Wang, 2005; see Iwasaki and Takahashi, 1998). The estimated distance between Ca^{2+} source and Ca^{2+} sensor at the BC-GC synapse is in the nanometer range, suggesting that coupling is mediated by protein-protein interactions (Berkefeld et al., 2006). Our results imply that these interactions must be highly specific, requiring both P/Q-type Ca^{2+} channels and specific reaction partners, presumably components of the release machinery of parvalbumin-expressing GABAergic interneurons. In contrast, coupling is loose in both cortical glutamatergic synapses in which a substantial proportion of release is mediated by P/Q-type channels (Reid et al., 2003; Ohana and Sakmann, 1998) and in GABAergic synapses of CCK-expressing interneurons in which release is exclusively mediated by N-type Ca^{2+} channels (Hefft and Jonas, 2005). One possibility is that P/Q-type Ca^{2+} channels couple directly to the Ca^{2+} sensor, presumably synaptotagmin (Südhof, 2002; Sheng et al., 1997). In this framework, synaptic specificity could be conferred by the selective expression of P/Q-type channels and distinct synaptotagmin isoforms. Consistent with this hypothesis, fast-spiking, parvalbumin-expressing BCs use a Ca^{2+} sensor different from synaptotagmin 1 (presumably synaptotagmin 2; A.M. Kerr et al., 2006, Soc. Neurosci., abstract). Alternatively, coupling may occur between synprint sites of Ca^{2+} channels and SNARE complex proteins (Rettig et al., 1996; Bezprozvanny et al., 2000; Mochida et al., 2003). In this scenario, specificity might be conferred by the selective expression of P/Q-type channels and distinct syntaxins or soluble NSF attachment proteins (SNAPs) in GABAergic interneurons (Verderio et al., 2004).

Tight coupling between Ca^{2+} inflow and transmitter release at BC-GC synapses will contribute to the fast signaling properties of BCs in multiple ways. First, tight coupling will increase the efficacy of GABAergic synaptic transmission. For a given number of presynaptic Ca^{2+} channels, increasing the coupling distance from 20 to 200 nm decreases the peak release rate by orders of magnitude (Figure 7F). Although this decrease in release probability could be compensated by an increase in the number of presynaptic Ca^{2+} channels, the physical size of the active zone places clear limits to the extent of any compensatory effects. Thus, tight coupling between Ca^{2+} source and Ca^{2+} sensor may explain the high probability of transmitter release at BC output synapses (Kraushaar and Jonas, 2000). Second, tight coupling will minimize the diffusional component of the synaptic delay (Meinrenken et al., 2002). In our model of Ca^{2+}-dependent transmitter release, increasing the coupling distance from 20 to 200 nm increases the synaptic delay by ~300 μs (Figure 7E). Thus, the coupling distance is a major determinant of the synaptic delay, which is <1 ms at room temperature. Third, tight coupling will increase the temporal precision of phasic release. Finally, tight coupling will increase the ratio of synchronous to asynchronous or ectopic release (Hefft and Jonas, 2005; Matsui and Jahr, 2004). Similarly, tight coupling may explain the lack of facilitation and potentiation at the BC-GC synapse (Kraushaar and Jonas, 2000; Tang et al., 2000; Awatramani et al., 2005; Zucker and Regehr, 2002). Thus, tight coupling between Ca^{2+} source and Ca^{2+} sensor extends the repertoire of rapid signaling mechanisms of fast-spiking, parvalbumin-expressing BCs (Jonas et al., 2004; Freund and Katona, 2007). As BCs are embedded in both feedback and feedforward inhibitory microcircuits, tight coupling will contribute to the speed and reliability of inhibition in the hippocampal network (Pouille and Scanziani, 2001, 2004). If tight coupling is a general property of BC output synapses, it will be also important for fast signaling at BC-BC synapses and the generation of fast network oscillations in interneuron networks (Bartos et al., 2007).

EXPERIMENTAL PROCEDURES

Pre-Embedding Immunoelectron Microscopy

Sections of the hippocampus of 2-month-old Wistar rats were processed for immunogold labeling (Baude et al., 1993; Kulik et al., 2004) with an affinity-purified polyclonal anti-α_{1A} antibody (Alomone Laboratories, Jerusalem, Israel). Briefly, animals were deeply anesthetized by Narkodorm-n (180 mg/kg, i.p.) (Alvetra, Neumünster, Germany), and perfused transcardially with 0.9% saline followed by fixative containing 4% paraformaldehyde, 15% saturated picric acid, and 0.05% glutaraldehyde in 0.1 M phosphate buffer (PB). Tissue blocks were washed in 0.1 M PB and 50 μm thick sections were cut on a vibratome. Sections were cryoprotected in a solution containing 25% sucrose and 10% glycerol in 50 mM PB and processed for pre-embedding immunogold labeling as described (Kulik et al., 2004). Serial ultrathin (70 nm) sections were cut from the surfaces of the samples. Axon terminals of putative parvalbumin-expressing interneurons were identified by their symmetric synaptic contacts with somata of dentate gyrus granule cells. Density of immunoparticles was quantified as the number of particles in the active zone versus the extrasynaptic membrane, divided by the corresponding surface areas.

Paired Recording

Transverse hippocampal slices (300 μm thickness) were cut from brains of 18- to 21-day-old Wistar rats using a vibratome. Animals were killed by decapitation, in agreement with national and institutional guidelines. Patch pipettes were pulled from thick-walled borosilicate glass tubing (2 mm outer diameter, 1 mm inner diameter); when filled with intracellular solution, the resistance was 2–3.5 MΩ. Simultaneous recordings from monosynaptically connected basket cells (BCs) and granule cells (GCs) in the dentate gyrus (Kraushaar and Jonas, 2000) were obtained under visual control using infrared differential interference contrast videomicroscopy. A tight-seal whole-cell recording was first established in a putative BC. Selected cells had somata located in the granule cell layer near the hilar border and generated >50 action potentials during 1 s depolarizing current pulses (600 pA to 1 nA). Subsequently, whole-cell recordings were made from GCs. To optimize the diffusional access to presynaptic terminals, paired recordings were made from adjacent cells with <100 μm intersomatic distance. The recording temperature was 22°C ± 2°C.

Two Axopatch 200A amplifiers (Axon Instruments) were used for recording. The presynaptic neuron was held in the current-clamp mode (I-clamp normal, holding potential −70 mV) and stimulated every 16 s. Action potentials were elicited by single or trains of current pulses (duration 1 ms, amplitude 1.4–2.4 nA). The postsynaptic cell was held in the voltage-clamp mode at a holding potential of −80 mV. Postsynaptic series resistance (range: 5–10 MΩ) was not compensated but was continuously monitored using a 4 mV test pulse; only pairs with <2 MΩ change were analyzed. Signals were filtered at 5 kHz (4-pole low-pass Bessel filter) and digitized at 10 kHz using a CED 1401plus interface (Cambridge Electronic Design). Pulse generation and data acquisition were performed using FPulse (U. Fröbe, Physiological Institute) running under Igor (version 5.03) on a PC. Morphology of pre- and postsynaptic neuron was visualized by post hoc staining, using 3,3′ diaminobenzidine as chromogen (Geiger et al., 1997).

Solutions

For storage of slices, a solution containing 87 mM NaCl, 25 mM $NaHCO_3$, 10 mM glucose, 75 mM sucrose, 2.5 mM KCl, 1.25 mM NaH_2PO_4, 0.5 mM $CaCl_2$, and 7 mM $MgCl_2$ (equilibrated with 95% O_2/5% CO_2 gas mixture) was used. For the experiments, the slices were superfused with physiological saline containing 125 mM NaCl, 25 mM $NaHCO_3$, 25 mM glucose, 2.5 mM KCl, 1.25 mM NaH_2PO_4, 2 mM $CaCl_2$ (or 0.5–4 mM $CaCl_2$ in a subset of experiments with replacement by sucrose as required), and 1 mM $MgCl_2$ (95% O_2/5% CO_2). The intracellular solution for the presynaptic neuron contained 135 mM Kgluconate, 20 mM KCl, 2 mM $MgCl_2$, 2 or 0.02 mM Na_2ATP, 0.5 mM NaGTP, 5 mM phosphocreatine, 10 mM HEPES, and 0.2 mg ml^{-1} biocytin. The intracellular solution for the postsynaptic neuron contained 110 mM KCl, 35 mM Kgluconate, 10 mM EGTA, 2 mM $MgCl_2$, 2 mM Na_2ATP, 10 mM HEPES, 1 mM QX-314, and 0.2 mg ml^{-1} biocytin; the pH was adjusted to 7.2 with KOH in both cases. In solutions in which chelators were added, the concentration of Kgluconate was reduced accordingly. Ethylenedioxybis-(o-phenylenenitrilo)tetraacetic acid (BAPTA) and ethyleneglycol-bis(2-aminoethylether)-N,N,N′,N′-tetraacetic acid (EGTA) were from Sigma, other chemicals were from Merck, Sigma, Riedel-de Haën, or Gerbu.

Pipette Perfusion

Ca^{2+} chelators were loaded into presynaptic BCs by pipette perfusion, using a custom-made two-port pipette holder and parts of the 2PK+ pipette perfusion kit (ALA Scientific Instruments, Westbury, NY). Presynaptic pipettes were filled with a small volume (2–4 μl) of intracellular solution. Chelators were applied through one port via a flexible quartz tubing (100 μm outer diameter) coated with polyamide. To minimize exchange times, the end of the tubing was positioned closely to the pipette tip. The other end was connected to an ~0.6 ml reservoir with chelator-containing solution. To deliver the chelators to the pipette, positive pressure was applied to the reservoir and a compensatory negative pressure was applied at the second port of the pipette holder (which was also used for suction during seal formation and transition from cell-attached into whole-cell mode). Both positive and negative pressure were generated by a pressure/vacuum pump system and controlled precisely using two independent regulators (2–5 mm Hg). Changes in electrode potential during perfusion were <2 mV for 30 mM of chelator. Recording time after the solution exchange was, on average, 85 ± 5 min (range: 47–179 min).

Control experiments with mock application of the original intracellular solution revealed that the rundown of evoked IPSCs during long-lasting recordings was small (to 80.4% of control value; Figure 4D and Figure S1D). Given the small extent of rundown, no correction was made. Control experiments were also performed to test whether presynaptic chelator concentrations might be affected by organic anion transporters (OATs). In two BC-GC pairs, we tested the effects of intracellular application of 30 mM EGTA after adding 1 mM of the OAT blocker probenecide to the bath solution. As the results were similar to those obtained in the absence of the drug, data were pooled. Finally, we tested whether the effects of exogenous chelators could be influenced by the expression of the endogenous Ca^{2+}-binding protein parvalbumin in BCs. In two BC-GC pairs from parvalbumin knockout (−/−) mice (Schwaller et al., 1999), we examined the effects of 30 mM EGTA applied via presynaptic patch pipette perfusion. The effects were similar to those obtained in wild-type rats (reduction of IPSC peak amplitude to 72.1% of control value). As the results were obtained from a different species, data were not included in the mean values.

To estimate the concentration of chelators reached in presynaptic terminals, diffusion from the soma into the BC axon was modeled with Neuron 5.9, using a mechanism based on COMPARTMENT and LONGITUDINAL_DIFFUSION (Carnevale and Hines, 2006). A previously described cable model of a dentate gyrus BC with fully reconstructed somatodendritic domain and main axon and schematically extended axonal arborization (150 collaterals) was used (Geiger et al., 1997). The diffusion coefficient for BAPTA and EGTA was assumed as 220 $\mu m^2\ s^{-1}$ (Naraghi and Neher, 1997) and the time step was 100 ms. These simulations indicated that the concentration at presynaptic terminals was close to that at the soma after 50–100 min recording times for proximal collaterals (Figure 2D).

Data Analysis

Data analysis was performed using Mathematica 4.1.2, 5.0, or 6.0.1 (Wolfram Research). Unitary IPSC peak amplitude was measured as the difference between baseline and the peak current <8 ms after the first presynaptic action potential. Stationarity of IPSC amplitudes was tested by Spearman rank correlation analysis with $p > 0.1$; only pairs fulfilling the stability criterion were used for subsequent analysis. Events were classified as successes when the amplitude was >3 standard deviations of the baseline noise and as failures otherwise. Coefficients of variation (CV, standard deviation/mean) of IPSC peak amplitudes were calculated from 30 traces during stationary control and test periods (Kraushaar and Jonas, 2000).

Modeling Chelator Effects with the Steady-State Solution to the Linearized Reaction-Diffusion Equations

Effects of Ca^{2+} chelators on synaptic transmission were modeled using the steady-state solution to the linearized reaction-diffusion problem obtained analytically (Neher, 1998). This approach assumed that buffer saturation is negligible. A vesicle carrying the Ca^{2+} sensor was either coupled to a single Ca^{2+} channel at variable distance r (single-channel model) or to a cluster of Ca^{2+} channels at variable distance d (cluster model). In the cluster model, d was measured from the center of the cluster, and the width of the cluster was quantified as the standard deviation σ of the normally distributed channel density. The ratio of Ca^{2+} transients in the presence and absence of chelators (R_{Ca}) was calculated as

$$R_{Ca} = (1/r\ \exp(-r/\lambda_b))/(1/r\ \exp(-r/\lambda_o))\ (\text{single channel}) \quad (1)$$

$$R_{Ca} = \left(\int n_{Ca}(r)\exp(-r/\lambda_b)dr\right) \Big/ \left(\int n_{Ca}(r)\exp(-r/\lambda_o)dr\right)(\text{cluster})\ \text{with} \quad (2)$$

$$\lambda_o = \sqrt{D_{Ca}/(k^o_{on}[B]^o)}\ \text{and} \quad (3)$$

$$\lambda_b = \sqrt{D_{Ca}/\left(k^o_{on}[B]^o + k^b_{on}B^b_T K^b_D/\left(\left[Ca^{2+}\right]_r + K^b_D\right)\right)}, \quad (4)$$

where r is radial distance, $n_{Ca}(r)$ is the Ca^{2+} channel density distribution, $\int$ is a definite integral (integration range 0–500 nm), D_{Ca} is the diffusion coefficient of free Ca^{2+}, k^o_{on} $[B]^o$ is the buffer product of endogenous buffer, k^b_{on} is the rate constant of Ca^{2+} binding to exogenous buffer, $[B]^b_T$ is the total concentration of exogenous buffer, K^b_D is the dissociation constant of exogenous buffer, and $[Ca^{2+}]_r$ is the resting Ca^{2+} concentration. Physicochemical properties of Ca^{2+} and chelators were assumed as follows (Naraghi and Neher, 1997; Neher, 1998; Nägerl et al., 2000): $D_{Ca} = 220\ \mu m^2\ s^{-1}$, $k^b_{on} = 4\ 10^8\ M^{-1}\ s^{-1}$ for BAPTA and $1\ 10^7\ M^{-1}\ s^{-1}$ for EGTA, and $K^b_D = 0.22\ \mu M$ for BAPTA and 0.07 μM for EGTA. Endogenous buffering properties of BCs were constrained based on measurement of Ca^{2+} transients in proximal dendrites of BCs (Y. Aponte et al., 2006, Soc. Neurosci., abstract). $[Ca^{2+}]_r$ was taken as the value previously measured with 100 μM fura-2 (71 nM), and k^o_{on} $[B]^o$ was determined as κ_S/τ (see Naraghi and Neher, 1997) = 202/0.2 s^{-1} = 1010 s^{-1}, where κ_S is the endogenous Ca^{2+} binding ratio of BCs (202) and τ is the fast decay time constant of the Ca^{2+} transients recorded with low concentrations of fura-2 or fura-FF (~200 ms; Y. Aponte, J. Bischofberger, and P.J., unpublished data; see Müller et al., 2007). The ratio of IPSCs in the presence and absence of

chelators (R_{IPSC}) was then calculated as $R_{IPSC} = f(R_{Ca})$, where f was the doubly normalized version of the power relation between transmitter release and extracellular [Ca^{2+}] at the BC-GC synapse (concentration normalized to 2 mM and release normalized to that at 2 mM; Figure 5C). Confidence intervals of r, d, and σ were obtained by bootstrap procedures. One thousand artificial data sets were generated from the means and SEMs of the original data set and were analyzed as the original (Efron and Tibshirani, 1998). Bootstrap procedures were also used to compare single-channel and cluster model with models in which Ca^{2+} channels were distributed more homogeneously (Figure 6B).

Time-Dependent Solution of the Full Reaction-Diffusion Equations and Simulation of Transmitter Release

To account for both possible deviations from the steady-state assumption and saturation of buffers, the time-dependent solution of the full reaction-diffusion equations was obtained numerically. This approach considered mobile and fixed buffers as well as buffer saturation. Assuming Ca^{2+} inflow at a point source and radial symmetry, the Ca^{2+} concentration as a function of time and radial distance can be obtained from a set of partial differential equations (Smith, 2001):

$$\frac{\partial\left[Ca^{2+}\right]}{\partial t} = D_{Ca}\frac{1}{r^2}\frac{\partial}{\partial r}\left(r^2\frac{\partial\left[Ca^{2+}\right]}{\partial r}\right) - \sum_i\left(k_{on,i}\left[Ca^{2+}\right][B_i] - k_{off,i}\left([B_i]_{tot}-[B_i]\right)\right) \quad (5a)$$

and

$$\frac{\partial[B_i]}{\partial t} = D_{B,i}\frac{1}{r^2}\frac{\partial}{\partial r}\left(r^2\frac{\partial[B_i]}{\partial r}\right) - \left(k_{on,i}\left[Ca^{2+}\right][B_i] - k_{off,i}\left([B_i]_{tot}-[B_i]\right)\right), \quad (5b)$$

where r is radial distance, t is time, [Ca^{2+}] is the free Ca^{2+} concentration, and $D_{Ca}$is the diffusion coefficient for Ca^{2+}. Furthermore, [B_i] is the free buffer concentration, $k_{on,i}$ the binding rate, $k_{off,i}$ the unbinding rate, $[B_i]_{tot}$ the total buffer concentration, and $D_{B,i}$ the diffusion coefficient of the ith buffer.

The boundary conditions near the source (corresponding to the region of the active zone) were given as

$$\lim\left(4\pi D_{Ca}r^2\frac{\partial\left[Ca^{2+}\right]}{\partial r}\right) = 2\sigma[t] \text{ for } r\rightarrow r_{min} \text{ and} \quad (6a)$$

$$\lim\left(4\pi D_{B,i}r^2\frac{\partial[B_i]}{\partial r}\right) = 0 \text{ for } r\rightarrow r_{min}, \quad (6b)$$

where σ[t] is the flux through the Ca^{2+} channels as a function of time, which was specified according to previous models of P/Q-type Ca^{2+} channels (Borst and Sakmann, 1998). The flux was multiplied by 2 to convert spherical into hemispherical symmetry. The peak amplitude was set to 1 pA, corresponding to <10 P/Q-type Ca^{2+} channels (Li et al., 2007). This amplitude value was chosen to approximately reproduce the experimentally observed relation between transmitter release and external Ca^{2+} concentration (Figure 5C) for a coupling distance of 20 nm.

The boundary conditions remote from the source (corresponding to the outer plasma membrane of the presynaptic terminal) were specified as

$$\lim\left(\frac{\partial\left[Ca^{2+}\right]}{\partial r}\right) = 0 \text{ for } r\rightarrow r_{max} \text{ and} \quad (7a)$$

$$\lim\left(\frac{\partial[B_i]}{\partial r}\right) = 0 \text{ for } r\rightarrow r_{max}. \quad (7b)$$

As the gradient is 0, no diffusion is possible beyond the outer boundary. Initial conditions were given as [Ca^{2+}] = 50 nM, with [B_i] being set to the corresponding equilibrium values. r_{min} and r_{max} were chosen as 1 nm and 500 nm, respectively.

The partial differential equation was solved using NDSolve of Mathematica 6.0.1, with a spatial grid resolution of <0.1 nm. Increasing the grid resolution by a factor of 3 had only minimal effects on the results. Diffusion coefficients were chosen $D_{Ca} = D_B = 220\ \mu m^2\ s^{-1}$. The affinities of mobile buffers (ATP) and endogenous fixed buffers were assumed as 200 and 2 μM, respectively, and the binding rates for Ca^{2+} were chosen as $5\ 10^8\ M^{-1}\ s^{-1}$ in both cases (Meinrenken et al., 2002). The concentration of mobile buffers was assumed as 290 μM (corresponding to 2 mM Mg ATP in the pipette solution; Meinrenken et al., 2002). The concentration of the fixed buffers was assumed as 160 μM, to account for the relatively high endogenous Ca^{2+} binding ratio of BCs (Y. Aponte et al., 2006, Soc. Neurosci., abstract). The ratio of IPSCs was calculated as $R_{IPSC} = f(R_{Ca})$, where R_{Ca} is the ratio of peak amplitudes of Ca^{2+} transients.

To simulate transmitter release for Ca^{2+} transients at various distances from the source, we used the previously published allosteric model of Ca^{2+}-dependent vesicle fusion (Lou et al., 2005). The model consisted of 12 states, 6 before and 6 after fusion. The Ca^{2+} binding rate was assumed as $k_{on} = 1\ 10^8\ M^{-1}\ s^{-1}$, the unbinding rate as $k_{off} = 4000\ s^{-1}$, and the basal fusion rate as $I_+ = 2\ 10^{-4}\ s^{-1}$. On and off rates were multiplied by integer numbers between 1 and 5 to implement independent Ca^{2+} binding at different sites. The cooperativity factors were chosen as b = 0.5 and f = 31.3 (Lou et al., 2005). The occupancies for the different states of the model were obtained by solving the corresponding first-order ordinary differential equation with a Q matrix approach. Finally, the release rate was obtained by differentiation of the sum of occupancies of all fused states.

Statistical Analysis

Values are given as means ± SEMs. Error bars in figures also indicate SEMs whenever they exceed the size of the symbols. Significance of differences was assessed by a nonparametric two-sided Wilcoxon signed rank test at the significance level (*P*) indicated.

Supplemental Data

The Supplemental Data for this article can be found online at http://www.neuron.org/cgi/content/full/57/4/■■■/DC1/.

ACKNOWLEDGMENTS

We thank Dr. J. Bischofberger for critically reading an earlier version of the manuscript; Dr. Arnd Roth for useful discussions; and S. Becherer, M. Northemann, and K. Winterhalter for technical assistance. Supported by the Deutsche Forschungsgemeinschaft (SFB 505, project C5, and Leibniz program).

Received: May 9, 2007
Revised: November 16, 2007
Accepted: December 26, 2007
Published: February 27, 2008

REFERENCES

Adler, E.M., Augustine, G.J., Duffy, S.N., and Charlton, M.P. (1991). Alien intracellular calcium chelators attenuate neurotransmitter release at the squid giant synapse. J. Neurosci. *11*, 1496–1507.

Augustine, G.J., Santamaria, F., and Tanaka, K. (2003). Local calcium signaling in neurons. Neuron *40*, 331–346.

Awatramani, G.B., Price, G.D., and Trussell, L.O. (2005). Modulation of transmitter release by presynaptic resting potential and background calcium levels. Neuron *48*, 109–121.

Bartos, M., Vida, I., and Jonas, P. (2007). Synaptic mechanisms of synchronized gamma oscillations in inhibitory interneuron networks. Nat. Rev. Neurosci. *8*, 45–56.

Baude, A., Nusser, Z., Roberts, J.D., Mulvihill, E., McIlhinney, R.A., and Somogyi, P. (1993). The metabotropic glutamate receptor (mGluR1α) is concentrated at perisynaptic membrane of neuronal subpopulations as detected by immunogold reaction. Neuron *11*, 771–787.

Berkefeld, H., Sailer, C.A., Bildl, W., Rohde, V., Thumfart, J.O., Eble, S., Klugbauer, N., Reisinger, E., Bischofberger, J., Oliver, D., et al. (2006). BK_{Ca}-Cav channel complexes mediate rapid and localized Ca^{2+}-activated K^+ signaling. Science *314*, 615–620.

Bezprozvanny, I., Zhong, P., Scheller, R.H., and Tsien, R.W. (2000). Molecular determinants of the functional interaction between syntaxin and N-type Ca^{2+} channel gating. Proc. Natl. Acad. Sci. USA *97*, 13943–13948.

Borst, J.G.G., and Sakmann, B. (1996). Calcium influx and transmitter release in a fast CNS synapse. Nature *383*, 431–434.

Borst, J.G.G., and Sakmann, B. (1998). Calcium current during a single action potential in a large presynaptic terminal of the rat brainstem. J. Physiol. *506*, 143–157.

Brandt, A., Khimich, D., and Moser, T. (2005). Few $Ca_V1.3$ channels regulate the exocytosis of a synaptic vesicle at the hair cell ribbon synapse. J. Neurosci. *25*, 11577–11585.

Carnevale, N.T., and Hines, M.L. (2006). The Neuron Book (Cambridge: Cambridge University Press).

Collin, T., Chat, M., Lucas, M.G., Moreno, H., Racay, P., Schwaller, B., Marty, A., and Llano, I. (2005). Developmental changes in parvalbumin regulate presynaptic Ca^{2+} signaling. J. Neurosci. *25*, 96–107.

Efron, B., and Tibshirani, R.J. (1998). An Introduction to the Bootstrap (London: Chapman and Hall/CRC).

Fedchyshyn, M.J., and Wang, L.Y. (2005). Developmental transformation of the release modality at the calyx of Held synapse. J. Neurosci. *25*, 4131–4140.

Freund, T.F., and Katona, I. (2007). Perisomatic inhibition. Neuron *56*, 33–42.

Geiger, J.R.P., Lübke, J., Roth, A., Frotscher, M., and Jonas, P. (1997). Submillisecond AMPA receptor-mediated signaling at a principal neuron-interneuron synapse. Neuron *18*, 1009–1023.

Hefft, S., and Jonas, P. (2005). Asynchronous GABA release generates long-lasting inhibition at a hippocampal interneuron–principal neuron synapse. Nat. Neurosci. *8*, 1319–1328.

Iwasaki, S., and Takahashi, T. (1998). Developmental changes in calcium channel types mediating synaptic transmission in rat auditory brainstem. J. Physiol. *509*, 419–423.

Jonas, P., Bischofberger, J., Fricker, D., and Miles, R. (2004). *Interneuron diversity series*: Fast in, fast out - temporal and spatial signal processing in hippocampal interneurons. Trends Neurosci. *27*, 30–40.

Kraushaar, U., and Jonas, P. (2000). Efficacy and stability of quantal GABA release at a hippocampal interneuron-principal neuron synapse. J. Neurosci. *20*, 5594–5607.

Kulik, A., Nakadate, K., Hagiwara, A., Fukazawa, Y., Luján, R., Saito, H., Suzuki, N., Futatsugi, A., Mikoshiba, K., Frotscher, M., and Shigemoto, R. (2004). Immunocytochemical localization of the α_{1A} subunit of the P/Q-type calcium channel in the rat cerebellum. Eur. J. Neurosci. *19*, 2169–2178.

Lee, S.-H., Rosenmund, C., Schwaller, B., and Neher, E. (2000). Differences in Ca^{2+} buffering properties between excitatory and inhibitory hippocampal neurons from the rat. J. Physiol. *525*, 405–418.

Li, L., Bischofberger, J., and Jonas, P. (2007). Differential gating and recruitment of P/Q-, N-, and R-type Ca^{2+} channels in hippocampal mossy fiber boutons. J. Neurosci. *27*, 13420–13429.

Lou, X., Scheuss, V., and Schneggenburger, R. (2005). Allosteric modulation of the presynaptic Ca^{2+} sensor for vesicle fusion. Nature *435*, 497–501.

Matsui, K., and Jahr, C.E. (2004). Differential control of synaptic and ectopic vesicular release of glutamate. J. Neurosci. *24*, 8932–8939.

Meinrenken, C.J., Borst, J.G.G., and Sakmann, B. (2002). Calcium secretion coupling at calyx of Held governed by nonuniform channel-vesicle topography. J. Neurosci. *22*, 1648–1667.

Mochida, S., Westenbroek, R.E., Yokoyama, C.T., Zhong, H., Myers, S.J., Scheuer, T., Itoh, K., and Catterall, W.A. (2003). Requirement for the synaptic protein interaction site for reconstitution of synaptic transmission by P/Q-type calcium channels. Proc. Natl. Acad. Sci. USA *100*, 2819–2824.

Müller, M., Felmy, F., Schwaller, B., and Schneggenburger, R. (2007). Parvalbumin is a mobile presynaptic Ca^{2+} buffer in the calyx of held that accelerates the decay of Ca^{2+} and short-term facilitation. J. Neurosci. *27*, 2261–2271.

Nägerl, U.V., Novo, D., Mody, I., and Vergara, J.L. (2000). Binding kinetics of calbindin-D_{28k} determined by flash photolysis of caged Ca^{2+}. Biophys. J. *79*, 3009–3018.

Naraghi, M., and Neher, E. (1997). Linearized buffered Ca^{2+} diffusion in microdomains and its implications for calculation of $[Ca^{2+}]$ at the mouth of a calcium channel. J. Neurosci. *17*, 6961–6973.

Neher, E. (1998). Usefulness and limitations of linear approximations to the understanding of Ca^{++} signals. Cell Calcium *24*, 345–357.

Ohana, O., and Sakmann, B. (1998). Transmitter release modulation in nerve terminals of rat neocortical pyramidal cells by intracellular calcium buffers. J. Physiol. *513*, 135–148.

Poncer, J.C., McKinney, R.A., Gähwiler, B.H., and Thompson, S.M. (1997). Either N- or P-type calcium channels mediate GABA release at distinct hippocampal inhibitory synapses. Neuron *18*, 463–472.

Pouille, F., and Scanziani, M. (2001). Enforcement of temporal fidelity in pyramidal cells by somatic feed-forward inhibition. Science *293*, 1159–1163.

Pouille, F., and Scanziani, M. (2004). Routing of spike series by dynamic circuits in the hippocampus. Nature *429*, 717–723.

Reid, C.A., Bekkers, J.M., and Clements, J.D. (2003). Presynaptic Ca^{2+} channels: a functional patchwork. Trends Neurosci. *26*, 683–687.

Rettig, J., Sheng, Z.H., Kim, D.K., Hodson, C.D., Snutch, T.P., and Catterall, W.A. (1996). Isoform-specific interaction of the α_{1A} subunits of brain Ca^{2+} channels with the presynaptic proteins syntaxin and SNAP-25. Proc. Natl. Acad. Sci. USA *93*, 7363–7368.

Rozov, A., Burnashev, N., Sakmann, B., and Neher, E. (2001). Transmitter release modulation by intracellular Ca^{2+} buffers in facilitating and depressing nerve terminals of pyramidal cells in layer 2/3 of the rat neocortex indicates a target cell-specific difference in presynaptic calcium dynamics. J. Physiol. *531*, 807–826.

Schwaller, B., Dick, J., Dhoot, G., Carroll, S., Vrbova, G., Nicotera, P., Pette, D., Wyss, A., Bluethmann, H., Hunziker, W., and Celio, M.R. (1999). Prolonged contraction-relaxation cycle of fast-twitch muscles in parvalbumin knockout mice. Am. J. Physiol. *276*, C395–C403.

Shahrezaei, V., Cao, A., and Delaney, K.R. (2006). Ca^{2+} from one or two channels controls fusion of a single vesicle at the frog neuromuscular junction. J. Neurosci. *26*, 13240–13249.

Sheng, Z.H., Yokoyama, C.T., and Catterall, W.A. (1997). Interaction of the synprint site of N-type Ca^{2+} channels with the C2B domain of synaptotagmin I. Proc. Natl. Acad. Sci. USA *94*, 5405–5410.

Smith, G.D. (2001). Modelling local and global calcium signals using reaction-diffusion equations. In Computational Neuroscience, E. de Schutter, ed. (Boca Raton, FL: CRC Press), pp. 49–85.

Stanley, E.F. (1993). Single calcium channels and acetylcholine release at a presynaptic nerve terminal. Neuron *11*, 1007–1011.

Stanley, E.F. (1997). The calcium channel and the organization of the presynaptic transmitter release face. Trends Neurosci. *20*, 404–409.

Südhof, T.C. (2002). Synaptotagmins: why so many? J. Biol. Chem. *277*, 7629–7632.

Tang, Y., Schlumpberger, T., Kim, T., Lueker, M., and Zucker, R.S. (2000). Effects of mobile buffers on facilitation: experimental and computational studies. Biophys. J. *78*, 2735–2751.

Verderio, C., Pozzi, D., Pravettoni, E., Inverardi, F., Schenk, U., Coco, S., Proux-Gillardeaux, V., Galli, T., Rossetto, O., Frassoni, C., and Matteoli, M. (2004). SNAP-25 modulation of calcium dynamics underlies differences in GABAergic and glutamatergic responsiveness to depolarization. Neuron *41*, 599–610.

Wilson, R.I., Kunos, G., and Nicoll, R.A. (2001). Presynaptic specificity of endocannabinoid signaling in the hippocampus. Neuron *31*, 453–462.

Zucker, R.S., and Regehr, W.G. (2002). Short-term synaptic plasticity. Annu. Rev. Physiol. *64*, 355–405.